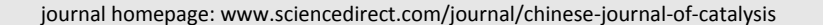


#### available at www.sciencedirect.com







# Article

# Electrocatalytic hydrogen evolution from water at low overpotentials with cobalt complexes supported by redox-active bipyridyl-NHC donors



Lizhu Chen<sup>†</sup>, Xiaojun Su<sup>†</sup>, Jonah W. Jurss<sup>\*</sup>

Department of Chemistry and Biochemistry, University of Mississippi, University, MS 38677, USA

#### ARTICLE INFO

Article history:
Received 1 April 2022
Accepted 12 July 2022
Available online 10 November 2022

Keywords:
Redox-active bipyridyl
N-heterocyclic carbene donors
Cobalt complex
Electrocatalysis
Water splitting
Hydrogen evolution

#### ABSTRACT

Three cobalt complexes bearing tunable, redox-active bipyridyl N-heterocyclic carbene (NHC)-based ligands have been studied for electrocatalytic hydrogen evolution from aqueous solutions. The effect of structural modifications to the ligand framework is investigated across the catalyst series, which includes a non-macrocyclic derivative (**1-Co**) and **16-(2-Co)** and **15-(3-Co)** membered macrocycles. A structure-activity relationship is demonstrated, in which the macrocyclic complexes have greater activity compared to their non-macrocyclic counterpart with the most rigid catalyst, supported by the **15**-membered macrocycle, performing best overall. Indeed, **3-Co** catalyzes  $H_2$  evolution from aqueous pH 4 acetate buffer with a Faradaic efficiency of 97% at a low overpotential of 330 mV. Mechanistic studies are consistent with formation of a cobalt-hydride species that is subsequently protonated to evolve  $H_2$  via a heterolytic pathway.

© 2022, Dalian Institute of Chemical Physics, Chinese Academy of Sciences.

Published by Elsevier B.V. All rights reserved.

# 1. Introduction

Energy consumption is a major driver of economic activity and has been linked with quality of life metrics [1]. However, global energy demand is predominantly met by burning fossil fuels, which is accompanied by greenhouse gas emissions and harmful environmental consequences [2]. Our reliance on these nonrenewable energy sources, i.e. coal, oil, and natural gas, can be reduced or potentially eliminated by developing clean energy fuel alternatives such as hydrogen. Indeed, solar energy or renewable electricity has been used to drive water splitting in artificial photosynthetic systems and electrolyzers [2–4]. In these devices, water oxidation at the anode is coupled to water (or proton) reduction at the cathode where hydrogen is evolved. The only byproduct of such a process is oxygen evolution at the anode.

Transition metal complexes have attracted significant attention as catalysts for the hydrogen evolution reaction (HER) because they are amenable to rational design, highly tunable, and conducive to mechanistic studies [5-16]. A number of Earth-abundant first-row transition metals have been employed for proton reduction in recent years, among which, cobalt-based catalysts have provided notable examples [17–47]. Cobalt catalysts bearing redox-active bipyridine- or pyrazine-based ligands have shown high activity and stability in water, but with relatively large overpotentials [26-37]. Tetraazamacrocycles, such as porphyrins, corroles, and diimine-dioxime frameworks, supporting cobalt have also been developed as competent catalysts for HER [34,35,38-46]. However, some diimine-dioxime based catalysts have been shown to possess low stability in acidic aqueous solutions limiting their practical implementation in large-scale water split-

 $<sup>\</sup>hbox{$^*$ Corresponding author. E-mail: jwjurss@olemiss.edu}\\$ 

<sup>†</sup> Contributed equally to this work.

ting technologies [45,48]. Related to the work presented here, Sakai and co-workers reported a cobalt complex bearing a macrocycle of alternating pyridyl and *N*-heterocyclic carbene (NHC) donors for photochemical hydrogen production in water, albeit with limited turnover numbers and a modest 65% conversion efficiency when driven with a chemical reductant [47].

Despite significant progress, existing HER catalysts are often restricted to organic solvents or water-organic mixtures due to poor solubility of the precatalyst and/or high overpotentials. Moreover, predictive design principles are often missing that would facilitate the rational development of more efficient catalysts. We recently reported a series of cobalt catalysts (Scheme 1) supported by highly tunable tetradentate ligands comprised of a redox-active 2,2'-bipyridyl moiety and electron-rich NHC donors [49,50], which were investigated for carbon dioxide reduction in both acetonitrile/2% H2O and aqueous solutions [49]. Although catalytic activity toward proton reduction was suppressed in the presence of CO<sub>2</sub>, electrochemical measurements indicated that the complexes may also be competent catalysts for proton reduction to H<sub>2</sub> [49]. Herein, we report the electrocatalytic activity of three Co complexes (Scheme 1) for the hydrogen evolution reaction in buffered aqueous solutions and in acetonitrile using dichloroacetic acid as the proton source.

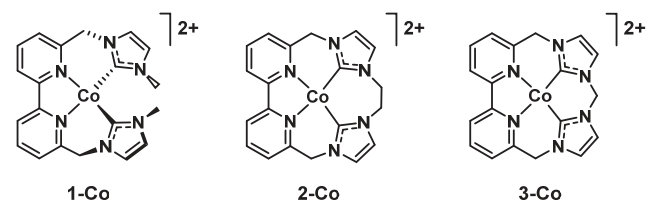
# 2. Experimental

#### 2.1. Materials

Anhydrous acetonitrile was distilled over  $CaH_2$  and stored over 4 Å molecular sieves before use. Water was purified by a Barnstead NANOpure Diamond water purification system. Buffer stock solutions were prepared by neutralizing 2.0 mol  $L^{-1}$  phosphoric acid and acetic acid solutions, respectively, with potassium hydroxide to the desired pH. All other chemicals used were ACS or reagent grade.

# 2.2. Electrochemical measurements

Electrochemistry was performed with a CH Instruments 600E Series potentiostat. Ohmic drop was compensated using the positive feedback compensation implemented by the system. Cyclic voltammetry was conducted in a three-electrode cell with a glassy carbon disk working electrode (3 mm dia.), a Ag/AgCl (3 mol L<sup>-1</sup> NaCl) reference electrode for aqueous solutions or a silver wire quasi–reference electrode for CH<sub>3</sub>CN solutions, and a platinum wire counter electrode. Nonaqueous cy-



**Scheme 1.** Cobalt(II) catalysts (**1-Co, 2-Co,** and **3-Co**) supported by tunable redox-active bipyridyl-NHC ligands.

clic voltammograms were referenced to the ferrocenium/ferrocene ( $Fc^{+/0}$ ) redox couple by adding ferrocene, as an internal standard, at the end of experiments. All cyclic voltammagrams were carried out under nitrogen atmosphere.

Controlled potential electrolyses were performed in a sealed two-chamber H-cell where the first chamber housed the Ag/AgCl reference electrode and a mercury pool electrode which was connected to the potentiostat via a glass-embedded platinum wire from the bottom. The other chamber held a high-surface area platinum mesh counter electrode. The two chambers were separated by a fine-porosity glass frit. For the working electrode chamber, the total volume is 263 mL, which includes 175 mL headspace, 80 mL solution, and 8 mL mercury. The diameter of the mercury pool is 4 cm. Solutions were purged with nitrogen gas for 30 min before electrolysis. Gas chromatography (Agilent 7890B Chromatograph and an Agilent PorapakQ (6' long, 1/8" O.D.) column) was used to quantify the evolved hydrogen at different time points during electrolysis. The amount of hydrogen was calculated by integrating the hydrogen peak and using a calibration curve which was generated from known standards purchased from BuyCal-Gas.com. Faradaic efficiencies were determined from the experimental amount of hydrogen generated during 2 h controlled potential electrolyses divided by the theoretical amount of hydrogen expected based on accumulated charge × 100.

#### 3. Results

The cobalt complexes were prepared as previously reported from the corresponding bipyridyl bis(imidazolium) salts [49]. Briefly, silver-NHC compounds were obtained by reacting the ligand precursors with excess Ag<sub>2</sub>O, which were subsequently transmetalated with CoCl2 and reacted with triflic acid to afford the cobalt(II) complexes as water-soluble triflate salts. With the cobalt complexes in hand, electrocatalytic proton reduction was investigated by cyclic voltammetry in aqueous acetate buffer (pH = 4) under  $N_2$  using a glassy carbon disk electrode. Substantial catalytic waves are observed with solutions containing the cobalt complexes, whereas reductive current in catalyst-free solutions or with added CoCl<sub>2</sub> (0.5 mmol L<sup>-1</sup>) is miniscule in comparison (Fig. 1(a)). For 1-Co, the catalytic response assigned to proton reduction appears at approximately -0.59 V vs. NHE. (The onset potential is reported where  $i_{cat} = 10$ μA on glassy carbon electrode.) CVs of 2-Co and 3-Co exhibit similar catalytic features, but with more negative onset potentials at around -0.65 and -0.61 V vs. NHE, respectively. We note that the rise in catalytic current is more shallow for **1-Co** compared to the macrocyclic systems. Further, the 15-membered macrocycle 3-Co exhibits a lower overpotential and greater activity relative to the less rigid, 16-membered macrocycle 2-Co. On this basis, the apparent overpotentials for hydrogen generation are less than 400 mV and significantly lower than that of most molecular HER catalysts in aqueous solutions, which often have overpotentials in excess of half a volt beyond the standard potential for proton reduction to H<sub>2</sub> (Table S1).

Cyclic voltammograms (CVs) of **1-Co**, **2-Co**, and **3-Co** show similar catalytic behavior and nearly equivalent onset poten-

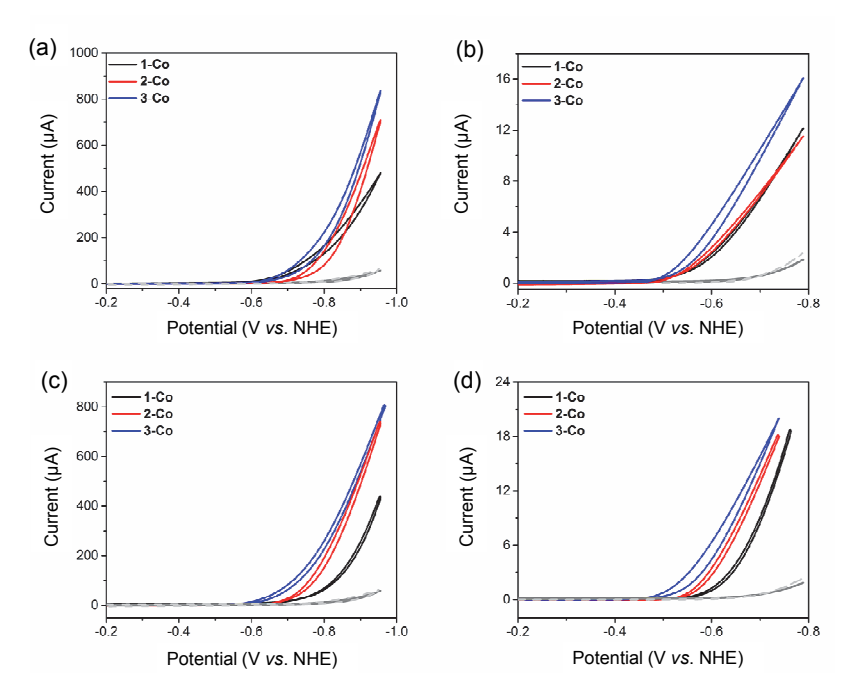


Fig. 1. (a) CVs of 0.5 mmol  $L^{-1}$  1-Co, 2-Co, and 3-Co in aqueous 0.5 mol  $L^{-1}$  acetate buffer (pH = 4) under  $N_2$  ( $\nu$  = 100 mV s<sup>-1</sup>, glassy carbon disk). (b) CVs of 5 μmol  $L^{-1}$  1-Co, 2-Co, and 3-Co in aqueous 1.0 mol  $L^{-1}$  pH 4 acetate buffer under  $N_2$  ( $\nu$  = 100 mV s<sup>-1</sup>, Hg pool (4 cm dia). (c) CVs under same conditions as graph (a), but immediately following a 60 s electrolysis at -0.8 V  $\nu$ s. NHE. (d) CVs under same conditions as graph (b), but immediately following a 60 s electrolysis at -0.6 V  $\nu$ s. NHE. CVs of electrode background and 0.5 mmol -0.6 U -0.6 V -0.6

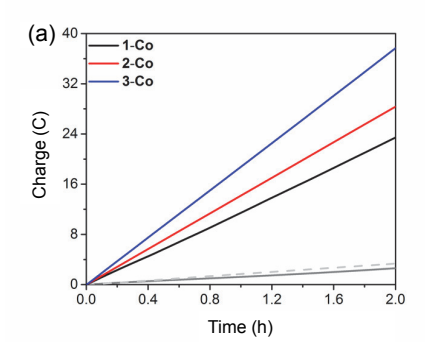
tials when changing the working electrode from glassy carbon to mercury (Fig. 1(b)). The onset potentials (reported at  $i_{\rm cat}$  = 0.3 mA on Hg pool electrode) at -0.48, -0.50, and -0.48 V vs. NHE for **1-Co**, **2-Co**, and **3-Co**, respectively, are positively shifted with respect to CVs obtained with a glassy carbon electrode. The electrode-dependent shift of 130 ( $\pm$  20) mV in onset potentials is presumably due to differences in catalyst-electrode interactions between the two electrode surfaces. Indeed, Kubiak, Batista, and coworkers showed that non-covalent London dispersion forces enhance electrocatalytic CO<sub>2</sub> reduction by nickel cyclam adsorbed to mercury electrodes [51]. This dispersive interaction caused flattening of the cyclam ligand which facilitates CO release from the catalyst [51].

Evidence of catalyst adsorption on both the glassy carbon and mercury electrodes was obtained by collecting CVs of each complex immediately after 60 s electrolyses at applied potentials corresponding to catalysis as shown in Figs. 1(c) and 1(d), respectively. The catalytic waves of 1-Co, 2-Co, and 3-Co were altered in comparing CVs before and after short-term electrolysis (Figs. S4-S6) with more significant changes observed on the mercury electrode relative to glassy carbon, consistent with the large (> 100 mV) positive shift in catalysis with Hg and a stronger catalyst-electrode interaction. Onset potentials for CVs following the 60 s electrolysis at a glassy carbon disk electrode (Fig. 1(d)) are -0.66, -0.64, and -0.58 V, and with a Hg pool electrode (Fig. 1(d)), -0.55, -0.53, and -0.47 V vs. NHE for 1-Co, **2-Co**, and **3-Co**, respectively. The relative ranking of catalysts on the basis of overpotential is clearly delineated after the electrolytic treatment, where catalysis occurs at progressively more positive voltages from 1-Co to 3-Co.

Relatively weak, reversible catalyst adsorption to the Hg electrode surface is apparent from the data in Figs. S4–S6 where stirring after the 60 s electrolyses reverts the current-potential profile back to its initial state, or nearly so. Plots of the catalytic current as a function of catalyst concentration show a linear dependence that reaches a plateau at concentrations of **1-Co**, **2-Co**, and **3-Co** exceeding 10, 6, and 6 µmol L<sup>-1</sup>, respectively (Figs. S7–S9). The limiting current obtained at concentrations beyond these values presumably reflects saturation conditions that correspond to monolayer surface coverage of the Hg surface.

To study the catalytic efficiency and stability of each catalyst, controlled potential electrolyses (CPEs) were performed in aqueous 1.0 mol L<sup>-1</sup> acetate buffer (pH 4) using an airtight two-compartment H-type electrochemical cell with a mercury pool working electrode. Gas chromatographic analysis of the headspace was used to quantify evolved hydrogen and determine Faradaic efficiencies. Despite the relatively low catalytic overpotentials and minor background current measured in CVs with a glassy carbon disk electrode, attempts at using a high surface area glassy carbon rod for CPE experiments were unsuccessful due to increasing background current instability versus time.

An applied potential of -0.57~V~vs. NHE was administered to each catalyst in order to compare catalytic activity across the series. Controlled potential electrolysis with **1-Co** in 1.0 mol L<sup>-1</sup> pH 4 acetate buffer showed catalytic current relative to background current in the absence of catalyst (Fig. 2(a)), consistent with its catalytic current response in CVs at -0.57~V~vs. NHE.



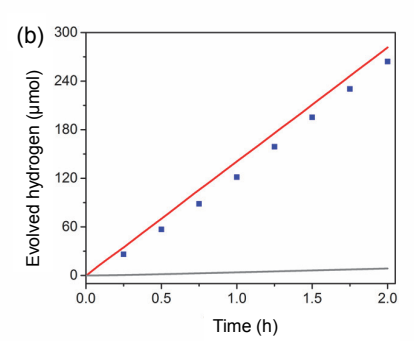


**Fig. 2.** (a) Charge vs. time plots from CPEs with 5 μmol  $L^{-1}$  **1-Co, 2-Co,** and **3-Co** in 1.0 mol  $L^{-1}$  pH 4 acetate buffer under  $N_2$ , applied potential ( $E_{appl}$ ) = -0.57 V vs. NHE, Hg pool (4 cm dia). Electrolyses of bare electrode and 0.5 mmol  $L^{-1}$  CoCl<sub>2</sub> under the same conditions are shown as gray and dashed gray curves, respectively. (b) Controlled potential electrolyses with (red) and without (gray) 5 μmol  $L^{-1}$  **3-Co** at  $E_{appl}$  = -0.57 V vs. NHE (same conditions, different CPE run than in Fig. 2(a)). The maximum theoretical  $H_2$  production is plotted (line) from accumulated charge. Blue squares are quantified  $H_2$  at different times points.

Likewise, charge-time profiles from CPEs with **2-Co** and **3-Co** demonstrate that the macrocyclic derivatives are also highly active under the same conditions (Fig. 2(a)). Indeed, the accumulated charge of 37.7 C for **3-Co** is more than those of **1-Co** and **2-Co**. Electrochemical data of the cobalt series is summarized in Table 1.

Nearly quantitative Faradaic efficiencies for evolved  $H_2$  were measured for all three catalysts (Table 1, Fig. 2(b)). The highest rate of  $H_2$  evolution was observed with **3-Co**, which reaches a turnover number (TON) of 472 after 2 h with no discernable loss of activity and a turnover frequency (TOF) of 236 h<sup>-1</sup> at -0.57 V vs. NHE. Indeed, the low overpotential (330 mV) and high catalytic activity of **3-Co** place it among the best molecular catalysts known for  $H_2$  evolution from water [6,8,9,12]. Tabulated data for representative earth-abundant homogeneous catalysts for aqueous proton reduction are provided in Table S1 for comparison.

The durability of **2-Co** and **3-Co** for electrocatalytic hydrogen generation was investigated by long-term controlled potential electrolyses. Steady current is passed over the course of 20 h as shown in Fig. S10, which suggests that both macrocyclic catalysts are highly stable under these conditions. Furthermore, CVs of **2-Co** and **3-Co** are essentially unchanged in wave shape and catalytic current before and after electrolysis (Fig. S11). A rinse test was performed on the used mercury pool electrode which showed no catalytic behavior (above background current) in fresh solutions without catalyst, suggesting that the molecular complexes do not generate a heterogeneous film or become irreversibly adsorbed to the electrode surface following electrolysis (Fig. S12). In addition, mercury can form an amalgam with cobalt which would be expected to poison the

surface of a nanoparticulate catalyst if present [52]. These results and the high Faradaic efficiencies indicate that **2-Co** and **3-Co** are robust molecular catalysts for H<sub>2</sub> evolution under these conditions.

Additional studies were conducted with **3-Co**, the best catalyst from the series, to gain insight into the mechanism for proton reduction to  $H_2$ . Electroanalytical Eq. (1) was applied to determine the relationship between catalytic current ( $i_{cat}$ ) and the concentrations of catalyst and substrate [53–55].

$$i_{cat} = n_{cat} FA[cat] \sqrt{Dk_{cat}[S]^{y}}$$
 (1)

In this expression,  $i_{cat}$  is the limiting catalytic current,  $n_{cat}$  is the electron stoichiometry of the catalytic reaction (2 for H+ reduction to H<sub>2</sub>), F is Faraday's constant, A is the area of the electrode surface, [cat] is the concentration of catalyst, D is the catalyst diffusion coefficient,  $k_{cat}$  is the catalytic rate constant, and [S] is the concentration of proton source. The dependence on catalyst concentration was probed by varying the concentration of **3-Co** in a series of CVs in pH = 4 acetate buffer using a glassy carbon disk electrode. Plots of catalytic current as a function of catalyst concentration give a linear dependence that begins to plateau at concentrations exceeding 200  $\mu$ mol L-1 (Fig. S13). A linear dependence is also obtained when switching the working electrode to mercury (Fig. S14). These results establish that the catalytic rate is first order in catalyst concentration and not dependent on the electrode material.

Next, cyclic voltammetry was performed in  $0.5 \text{ mol L}^{-1}$  buffered aqueous solutions to vary the pH from 2 to 8 using phosphate or acetate buffer. As shown in Fig. 3, the catalytic wave with **3-Co** shifts linearly to more positive potentials with decreasing pH values. The slope obtained in a plot of potential (at 1 mA of current) versus pH is  $\sim 60 \text{ mV pH}^{-1}$ , indicative of a

**Table 1** Experimental results for **1-Co**, **2-Co**, and **3-Co** from cyclic voltammetry and 2-h controlled potential electrolyses ( $E_{appl} = -0.57 \text{ V vs. NHE}$ ) in 1.0 mol L<sup>-1</sup> pH 4 acetate buffer under N<sub>2</sub> at a Hg pool electrode (4 cm dia).

Catalyst	E <sub>cat</sub> <sup>a</sup> (V)	E <sub>cat</sub> b (V)	Charge (C)	FE (%)	TON c	TOF (h-1)
1-Co	-0.66	-0.55	23.4	100	295	147
2-Co	-0.64	-0.53	28.4	97	358	179
3-Со	-0.58	-0.47	37.7	97	472	236

<sup>&</sup>lt;sup>a</sup>Onset potentials from CVs (Fig. 1(c)) at  $i_{cat}$  = 10  $\mu$ A (glassy carbon disk). <sup>b</sup>Onset potentials from CVs (Fig. 1(d)) at  $i_{cat}$  = 0.3 mA (Hg pool). <sup>c</sup>TON values determined from the 2 h electrolyses shown in Fig. 2(a).

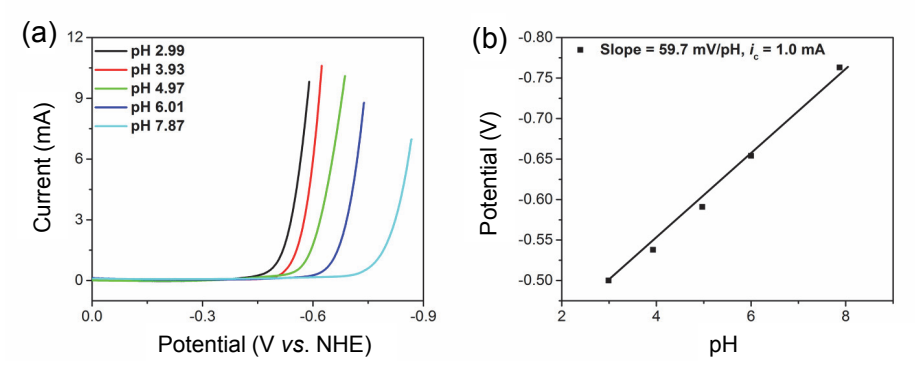


Fig. 3. (a) CVs of 5  $\mu$ mol L<sup>-1</sup> 3-Co in 1.0 mol L<sup>-1</sup> buffered aqueous solutions at different pH under N<sub>2</sub> at  $\nu$  = 100 mV s<sup>-1</sup>, Hg pool electrode. (b) Plot of the catalytic potential at  $i_{cat}$  = 1 mA (black) as a function of pH.

proton-coupled reduction involving 1e- and 1H+ [56].

The catalytic activity of **3-Co** was also investigated in nonaqueous conditions with dichloroacetic acid as the proton source, which has a p $K_a$  of 13.2 in acetonitrile and an appropriate reduction potential ( $E^o_{HA} = -0.92 \text{ V} vs. \text{ Fc}^{+/0}$ )<sup>57</sup> relative to the first reduction of **3-Co** at  $E_{1/2} = -1.31 \text{ V}$  (Fig. S15). Cyclic voltammetry with **3-Co** was initially conducted in the absence of substrate in anhydrous acetonitrile (CH<sub>3</sub>CN) containing 0.1 mol L<sup>-1</sup> Bu<sub>4</sub>NPF<sub>6</sub> as the supporting electrolyte. In contrast to the surface adsorption observed in aqueous solutions, CVs at different scan rates in acetonitrile show that the cathodic peak currents ( $i_p$ ) vary linearly with  $v^{1/2}$  (Fig. S15), consistent with a diffusion-controlled redox process. We note that analogous scan rate dependent CVs demonstrate that **1-Co** and **2-Co** are also freely diffusing under these conditions (Figs. S16 and S17).

The addition of dichloroacetic acid to **3-Co** triggers a large catalytic wave around -1.3 V vs. Fc+/0 as shown in Fig. 4(a). To determine the reaction order with respect to the proton source, CVs with **3-Co** were obtained in which the concentration of dichloroacetic acid was varied incrementally. A plot of catalytic current ( $i_{cat}$ ) as a function of acid concentration reveals a linear dependence at initial concentrations that begins to plateau at  $\sim$ 30 mmol L-1 dichloroacetic acid, indicative of saturation conditions (Fig. 4(b)). CVs with various concentrations of **3-Co** were also conducted in CH<sub>3</sub>CN/0.1 mol L-1 Bu<sub>4</sub>NPF<sub>6</sub> solutions containing 50 mmol L-1 dichloroacetic acid, revealing a linear dependence on catalytic current as a function of catalyst con-

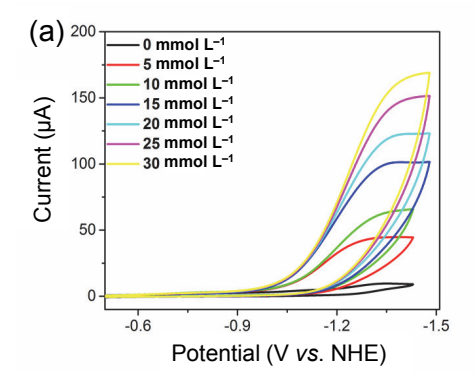
centration. From these experiments and applying Eq. (1), the linear relationships observed in plots of  $i_{cat}$  versus [3-Co] and  $i_{cat}$  versus dichloroacetic acid concentration (up to  $\sim$ 30 mmol L<sup>-1</sup>) demonstrate that catalysis is first order in catalyst and second order in acid ([S]) where y=2 in the expression.

The observed rate constant for **3-Co**-catalyzed proton reduction was also evaluated by cyclic voltammetry from  $CH_3CN/0.1$  mol  $L^{-1}$  BuNPF<sub>6</sub> solutions containing dichloroacetic acid using Eq. (2) [19].

$$\frac{i_{cat}}{i_p} = \frac{n_{cat}}{0.4463} \sqrt{\frac{RTk_{cat} [H^+]^2}{Fv}}$$
 (2)

Here,  $i_{\rm p}$  is the reduction peak current in the absence of acid, R is the ideal gas constant, T is the temperature,  $k_{\rm cat}$  is the observed rate constant for the catalytic reaction, and  $\nu$  is the scan rate. Plotting the ratio  $i_{\rm cat}/i_{\rm p}$  versus [acid] displays linear behavior as a function of scan rate (Fig. S18) [19]. The slopes obtained from Fig. S18 were plotted versus the inverse square root of the scan rate ( $\nu^{-1/2}$ ), which produces a slope of 0.744 (Fig. S19) that corresponds to a catalytic rate constant of ~1 L mol<sup>-1</sup> s<sup>-1</sup> and a calculated TOF of 36 mol H<sub>2</sub>/(mol 3-Co × h) with 100 mmol L<sup>-1</sup> dichloroacetic acid.

Likewise, we sought to compare the activity of the macrocyclic catalysts **2-Co** and **3-Co** under these conditions, CVs of **2-Co** were performed in the presence of dichloroacetic acid. However, the catalytic activity overlaps with the background proton reduction of the glassy carbon electrode itself (Fig. S20), preventing a direct comparison of the two catalysts and clearly



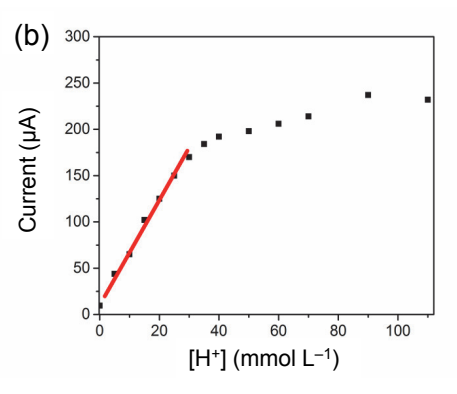


Fig. 4. (a) CVs of 1 mmol  $L^{-1}$  3-Co in anhydrous  $CH_3CN/0.1$  mol  $L^{-1}$   $Bu_4NPF_6$  solution with various concentrations of dichloroacetic acid (glassy carbon disk, v = 100 mV  $s^{-1}$ ). (b) Plot of catalytic current vs. acid concentration.

demonstrating the superiority of **3-Co**.

#### 4. Discussion

There are no observable reductive features prior to the catalytic wave associated with each cobalt catalyst in aqueous solution. Previous electronic structure calculations of the reduced cobalt complexes indicate that the first reduction, coincident with the catalytic activity observed here, is localized on the bipyridine moiety of the ligand framework for all three catalysts [49]. By virtue of its coordination, the bipyridine donor is strongly coupled to the metal center and the cobalt metal center is expected to react with a proton to form a cobalt(III)-hydride assuming catalysis is triggered by the 1e<sup>-</sup> reduced species. In general, metal-hydride species are key intermediates in catalytic cycles for the hydrogen evolution reaction involving transition metal-based catalysts [5–16].

Interestingly, CO<sub>2</sub> reduction with this series is initiated at the second reduction of these catalysts in acetonitrile solutions (0.1 mol L-1 Bu<sub>4</sub>NPF<sub>6</sub>) containing 2% H<sub>2</sub>O [49]. While the catalysts are highly selective for CO2-to-CO conversion, small amounts of H2 are produced under these conditions with no current enhancement observed at the first reduction. In addition, computed free energy profiles for protonation of the neutral 2e- reduced catalysts by a (H2O)5 cluster to form Co(II)-hydride intermediates revealed activation energies ( $\Delta G^{\dagger}$ ) of 26.0, 23.4, and 22.7 kcal mol-1 for 1-Co, 2-Co, and 3-Co, respectively [49]. The calculations suggest that the cobalt center becomes more nucleophilic across the series as the second reduction favors a metal-localized process. An explanation for the difference in reactivity observed at the first reduction versus the second reduction (which occurs at -2.03 V vs. Fc+/0 for **3-Co)** [49] in acetonitrile is that the strongest acid present in CO<sub>2</sub>-saturated CH<sub>3</sub>CN/2% H<sub>2</sub>O solutions is expected to be carbonic acid (p $K_a$  = 17.03 in CH<sub>3</sub>CN) [58], which is a weaker proton donor than dichloroacetic acid.

From the experimental results reported here, the rate-limiting step for 3-Co is first order in catalyst and second order in proton source (as measured in nonaqueous conditions). In aqueous solutions, catalysis is pH-dependent and varies with a slope consistent with a  $1\text{e-}/1\text{H}^+$  process. Given the second-order dependence on acid, the metal-hydride intermediate is presumably reduced and reacts with a second proton to liberate  $H_2$  and resume the catalytic cycle. Assuming a consistent mechanism in both  $CH_3CN$  and aqueous solutions, we hypothesize that the second step is a rate-limiting proton-coupled reduction, which is responsible for the observed pH dependence.

# 5. Conclusions

We have investigated a series of molecular cobalt electrocatalysts comprised of a redox-active bipyridine moiety and NHC donors that are active for HER in acidic acetate-buffered aqueous solutions. The results show that small changes to the tetradentate framework have a significant impact on reactivity and overpotential. Faradaic efficiencies for hydrogen evolution are nearly quantitative across the series and a dramatic difference in overpotentials is found in comparing non-macrocyclic complex **1-Co** to its macrocyclic counterparts **2-Co** and **3-Co**. The most rigid 15-membered macrocycle supporting **3-Co** affords the best catalyst, which evolves hydrogen from aqueous protons with a TOF of 236 h<sup>-1</sup> at a low overpotential of 330 mV. Mechanistic studies suggest that catalysis proceeds through a cobalt-hydride intermediate that is subsequently protonated to release H<sub>2</sub>.

# **Electronic supporting information**

Supporting information is available in the online version of this article.

Materials and methods, synthesis and characterization of

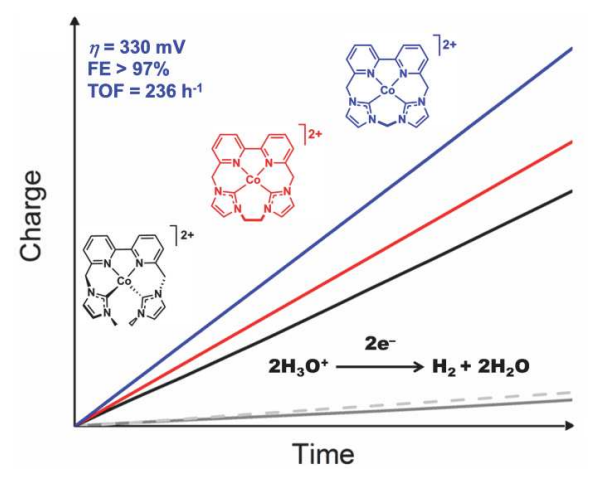
# **Graphical Abstract**

Chin. J. Catal., 2022, 43: 3187–3194 doi: 10.1016/S1872-2067(22)64151-2

Electrocatalytic hydrogen evolution from water at low overpotentials with cobalt complexes supported by redox-active bipyridyl-NHC donors

Lizhu Chen, Xiaojun Su, Jonah W. Jurss \* *University of Mississippi, USA* 

Three cobalt complexes bearing tunable, redox-active bipyridyl-*N*-heterocyclic carbine-based ligands are studied for electrocatalytic hydrogen evolution from aqueous solutions. High Faradaic efficiencies at low overpotentials are achieved, and a structure-activity relationship is revealed where the smallest macrocycle performs best overall.



imidazolium ligand precursors, electrochemical results, tabulated data of selected Earth-abundant molecular electrocatalysts for hydrogen evolution in aqueous solutions.

# **Notes**

The authors declare no competing financial interests. †These authors contributed equally to this work.

# Acknowledgments

We thank the National Science Foundation for generous funding through a CAREER award (CHE-1848478).

# References

- [1] Ö. Esen, M. Bayrak, J. Econ. Finac. Admin. Sci., 2017, 22, 75-98.
- [2] N. S. Lewis, D. G. Nocera, Proc. Natl. Acad. Sci. U. S. A., 2006, 103, 15729–15735.
- [3] D. Gust, T. A. Moore, A. L. Moore, Acc. Chem. Res., 2009, 42, 1890–1898.
- [4] S. Berardi, S. Drouet, L. Francàs, C. Gimbert-Suriñach, M. Guttentag, C. Richmond, T. Stoll, A. Llobet, *Chem. Soc. Rev.*, **2014**, 43, 7501–7519.
- [5] J. L. Dempsey, B. S. Brunschwig, J. R. Winkler, H. B. Gray, *Acc. Chem. Res.*, 2009, 42, 1995–2004.
- [6] V. Artero, M. Chavarot-Kerlidou, M. Fontecave, *Angew. Chem. Int. Ed.*, 2011, 50, 7238–7266.
- [7] P. Du, R. Eisenberg, Energy Environ. Sci., 2012, 5, 6012–6021.
- [8] M. Wang, L. Chen, L. Sun, Energy Environ. Sci., 2012, 5, 6763-6778.
- [9] V. S. Thoi, Y. Sun, J. R. Long, C. J. Chang, Chem. Soc. Rev., 2013, 42, 2388–2400.
- [10] W. T. Eckenhoff, W. R. McNamara, P. Du, R. Eisenberg, *Biochim. Biophys. Acta*, 2013, 1827, 958–973.
- [11] R. M. Bullock, A. M. Appel, M. L. Helm, Chem. Commun., 2014, 50, 3125–3143.
- [12] N. Queyriaux, R. T. Jane, J. Massin, V. Artero, M. Chavarot-Kerlidou, Coord. Chem. Rev., 2015, 304–305, 3–19.
- [13] D. Z. Zee, T. Chantarojsiri, J. R. Long, C. J. Chang, Acc. Chem. Res., 2015, 48, 2027–2036.
- [14] K. Mase, S. Aoi, K. Ohkubo, S. Fukuzumi, J. Porphyrins Phthalocyanines, 2016, 20, 935–949.
- [15] L. Tong, L. Duan, A. Zhou, R. P. Thummel, Coord. Chem. Rev., 2020, 402, 213079.
- [16] X. Li, H. Lei, L. Xie, N. Wang, W. Zhang, R. Cao, Acc. Chem. Res., 2022, 55, 878–892.
- [17] V. Houlding, T. Geiger, U. Kölle, M. Grätzel, J. Chem. Soc., Chem. Commun., 1982, 681–683.
- [18] P. V. Bernhardt, L. A. Jones, *Inorg. Chem.*, **1999**, 38, 5086–5090.
- [19] J. P. Bigi, T. E. Hanna, W. H. Harman, A. Chang, C. J. Chang, *Chem. Commun.*, 2010, 46, 958–960.
- [20] B. D. Stubbert, J. C. Peters, H. B. Gray, J. Am. Chem. Soc., 2011, 133, 18070–18073.
- [21] W. R. McNamara, Z. Han, C.-J. Yin, W. W. Brennessel, P. L. Holland, R. Eisenberg, *Proc. Natl. Acad. Sci. U. S. A.*, **2012**, 109, 15594–15599.
- [22] P. Zhang, M. Wang, F. Gloaguen, L. Chen, F. Quentel, L. Sun, Chem. Commun., 2013, 49, 9455–9457.
- [23] L. Chen, M. Wang, K. Han, P. Zhang, F. Gloaguen, L. Sun, *Energy Environ. Sci.*, 2014, 7, 329–334.
- [24] D. Basu, S. Mazumder, X. Shi, H. Baydoun, J. Niklas, O. Poluektov, H.

- B. Schlegel, C. N. Verani, *Angew. Chem. Int. Ed.*, **2015**, 54, 2105–2110.
- [25] C. R. Carr, A. Taheri, L. A. Berben, J. Am. Chem. Soc., 2020, 142, 12299–12305.
- [26] W. M. Singh, T. Baine, S. Kudo, S. Tian, X. A. N. Ma, H. Zhou, N. J. DeYonker, T. C. Pham, J. C. Bollinger, D. L. Baker, B. Yan, C. E. Webster, X. Zhao, *Angew. Chem. Int. Ed.*, 2012, 51, 5941–5944.
- [27] M. Guttentag, A. Rodenberg, C. Bachmann, A. Senn, P. Hamm, R. Alberto, *Dalton Trans.*, 2012, 42, 334–337.
- [28] C.-F. Leung, S.-M. Ng, C.-C. Ko, W.-L. Man, J. Wu, L. Chen, T.-C. Lau, Energy Environ. Sci., 2012, 5, 7903–7907.
- [29] L. Tong, R. Zong, R. P. Thummel, J. Am. Chem. Soc., 2014, 136, 4881–4884.
- [30] M. Nippe, R. S. Khnayzer, J. A. Panetier, D. Z. Zee, B. S. Olaiya, M. Head-Gordon, C. J. Chang, F. N. Castellano, J. R. Long, *Chem. Sci.*, 2013, 4, 3934–3945.
- [31] R. S. Khnayzer, V. S. Thoi, M. Nippe, A. E. King, J. W. Jurss, K. A. El Roz, J. R. Long, C. J. Chang, F. N. Castellano, *Energy Environ. Sci.*, 2014, 7, 1477–1488.
- [32] J. W. Jurss, R. S. Khnayzer, J. A. Panetier, K. A. E. Roz, E. M. Nichols, M. Head-Gordon, J. R. Long, F. N. Castellano, C. J. Chang, *Chem. Sci.*, 2015. 6, 4954–4972.
- [33] L. Chen, A. Khadivi, M. Singh, J. W. Jurss, *Inorg. Chem. Front.*, 2017, 4, 1649–1653.
- [34] E. Joliat, S. Schnidrig, B. Probst, C. Bachmann, B. Springler, K. K. Baldridge, F. von Rohr, A. Schilling, R. Alberto, *Dalton Trans.*, 2016, 45, 1737–1745.
- [35] L. Kohler, J. Niklas, R. C. Johnson, M. Zeller, O. G. Poluektov, K. L. Mulfort, *Inorg. Chem.*, 2019, 58, 1697–1709.
- [36] N. Queyriaux, D. Sun, J. Fize, J. Pécaut, M. J. Field, M. Chava-rot-Kerlidou, V. Artero, J. Am. Chem. Soc., 2020, 142, 274–282.
- [37] P. Wang, G. Liang, N. Smith, K. Hill, B. Donnadieu, C. E. Webster, X. Zhao, *Angew. Chem. Int. Ed.*, 2020, 59, 12694–12697.
- [38] R. M. Kellett, T. G. Spiro, *Inorg. Chem.*, **1985**, 24, 2373–2377.
- [39] B. B. Beyene, S. B. Mane, C.-H. Hung, Chem. Commun., 2015, 51, 15067–15070.
- [40] L. Xie, J. Tian, Y. Ouyang, X. Guo, W. Zhang, U.-P. Apfel, W. Zhang, R. Cao, Angew. Chem. Int. Ed., 2020, 59, 15844–15848.
- [41] B. Mondal, K. Sengupta, A. Rana, A. Mahammed, M. Botoshansky, S. G. Dey, Z. Gross, A. Dey, *Inorg. Chem.*, 2013, 52, 3381–3387.
- [42] X. Guo, N. Wang, X. Li, Z. Zhang, J. Zhao, W. Ren, S. Ding, G. Xu, J. Li, U.-P. Apfel, W. Zhang, R. Cao, *Angew. Chem. Int. Ed.*, **2020**, 59, 8941–8946.
- [43] X. Li, B. Lv, X.-P. Zhang, X. Jin, K. Guo, D. Zhou, H. Bian, W. Zhang, U.-P. Apfel, R. Cao, Angew. Chem. Int. Ed., 2022, 61, e202114310.
- [44] C. Baffert, V. Artero, M. Fontecave, *Inorg. Chem.*, 2007, 46, 1817–1824.
- [45] X. Hu, B. M. Cossairt, B. S. Brunschwig, N. S. Lewis, J. C. Peters, Chem. Commun., 2005, 4723–4725.
- [46] C. C. L. McCrory, C. Uyeda, J. C. Peters, J. Am. Chem. Soc., 2012, 134, 3164–3170.
- [47] K. Kawano, K. Yamauchi, K. Sakai, Chem. Commun., 2014, 50, 9872–9875.
- [48] N. Kaeffer, A. Morozan, J. Fize, E. Martinez, L. Guetaz, V. Artero, ACS Catal., 2016, 6, 3727–3737.
- [49] X. Su, K. M. McCardle, L. Chen, J. A. Panetier, J. W. Jurss, ACS Catal., 2019, 9, 7398–7408.
- [50] X. Su, K. M. McCardle, J. A. Panetier, J. W. Jurss, Chem. Commun., 2018. 54, 3351–3354.
- [51] Y. Wu, B. Rudshteyn, A. Zhanaidarova, J. D. Froehlich, W. Ding, C. P. Kubaik, V. S. Batista, ACS Catal., 2017, 7, 5282–5288.
- [52] J. L. Alvarez-Hernandez, J. W. Han, A. E. Sopchak, Y. Guo, K. L. Bren,

ACS Energy Lett., 2021, 6, 2256-2261.

- [53] J. M. Saveant, E. Vianello, *Electrochim. Acta*, **1963**, 8, 905–923.
- [54] R. S. Nicholson, I. Shain, Anal. Chem., 1964, 36, 706-723.
- [55] E. S. Rountree, B. D. McCarthy, T. T. Eisenhart, J. L. Dempsey, *Inorg. Chem.*, 2014, 53, 9983–10002.
- [56] D. R. Weinberg, C. J. Gagliardi, J. F. Hull, C. F. Murphy, C. A. Kent, B. C. Westlake, A. Paul, D. H. Ess, D. G. McCafferty, T. J. Meyer, Chem.

Rev., 2012, 112, 4016-4093.

- [57] G. A. N. Felton, R. S. Glass, D. L. Lichtenberger, D. H. Evans, *Inorg. Chem.*, 2006, 45, 9181–9184.
- [58] M. H. Rønne, D. Cho, M. R. Madsen, J. B. Jakobsen, S. Eom, E. Escoudé, H. C. D. Hammershøj, D. U. Nielsen, S. U. Pedersen, M.-H. Baik, T. Skrydstrup, K. Daasbjerg, J. Am. Chem. Soc., 2020, 142, 4265–4275.

# 氧化还原活性联吡啶N-杂环卡宾供体负载的钴配合物在低过电位下电催化水析氢

Lizhu Chen <sup>†</sup>, Xiaojun Su <sup>†</sup>, Jonah W. Jurss <sup>\*</sup>

密西西比大学化学与生物化学系,密西西比,美国

摘要:本文研究了三种可调的、具有氧化还原活性联吡啶-N-杂环卡宾(NHC)配体的钴配合物水溶液的电催化析氢性能.考察了在整个催化剂体系中结构修饰对配体框架的影响,其中包括非大环衍生物(1-Co)和16(2-Co)和15元大环(3-Co).结构-活性关系研究结果表明,大环-环状络合物的活性高于非大环络合物,其中最刚性的15元大环负载的催化剂整体性能最佳.在330 mV的低过电位下,3-Co催化pH=4的醋酸盐缓冲液析氢反应的法拉第效率为97%.机理研究与钴氢化物物种的形成相吻合,钴氢化物会质子化,并通过杂化方式放出H<sub>2</sub>.

关键词: 氧化还原活性联吡啶; N-杂环卡宾供体; 钴配合物; 电催化; 水分解; 析氢反应

收稿日期: 2022-04-01. 接受日期: 2022-07-12. 上网时间: 2022-11-10.

\*通讯联系人. 电子信箱: jwjurss@olemiss.edu

\*共同第一作者

基金来源: 国家科学基金(CHE-1848478).

本文的电子版全文由Elsevier出版社在ScienceDirect上出版(http://www.sciencedirect.com/journal/chinese-journal-of-catalysis).